ORIGINAL PAPER

Regional attributes of hurricane surge response functions for hazard assessment

Youn Kyung Song · Jennifer L. Irish · Ikpoto E. Udoh

Abstract Accurate quantification of hurricane surge probabilities is critically important for coastal planning and design. Recently, the joint probability method has been shown to yield statistically reliable surge probabilities and has quickly become the method of choice for extreme-value surge analysis in the United States. A main disadvantage of the joint probability method is the requirement to have accurate computational surge simulations for a large array of hurricane conditions. Recently, this shortcoming has been overcome by using a variety of interpolation schemes to reduce the number of surge simulations required to an optimal sample for joint probability analysis. One interpolation scheme uses response functions, or physically based dimensionless scaling laws, that consider the relative impact of hurricane landfall position, central pressure, and storm size on surge magnitude at the location of interest. Here, the influence of regional changes in bathymetry on the physically based response function form is investigated. It will be shown that the influence of continental shelf width on surge generation along a continuous coast is coupled with the influence of storm size and that this coupled physical effect can be treated within the response functions via dimensionless scaling. The surge response function model presented here has an algebraic form for rapid calculation. This model performs well for the entire 600-km Texas coast, yielding accurate surge estimates (root-mean-square errors less than 0.22 m and R^2 correlations better than 0.97) with virtually no bias (mean error magnitudes less than 0.03 m).

Keywords Storm surge · Coastal flooding · Tropical cyclones · Hurricanes · Risk assessment

List of symbols

JPM-OS	Joint probability method with optimal sampling
NOAA	National Oceanic and Atmospheric Administration

Y. K. Song · I. E. Udoh
Department of Civil Engineering, Texas A&M University, College Station, TX 77843-3136, USA

J. L. Irish (✉)
Department of Civil and Environmental Engineering, Virginia Tech, Blacksburg, VA 24061, USA
e-mail: jirish@vt.edu

PBL	Planetary boundary layer
SLR	Sea-level rise
SRF	Surge response function
H	Heaviside function where $H(y) = 1$ when $y \geq 0$ and $H(y) = 0$ when $y < 0$
L_{30}	Cross-shore distance between the shoreline and the 30-m depth contour
P_{far}	Far-field barometric pressure
R_p	Hurricane pressure radius near landfall
R_{thres}	Threshold value of R_p
T_R	Return period
c	Dimensionless regional scaling constant
c_p	Hurricane central pressure near landfall
$c_{p\text{-max}}$	Constant minimum possible hurricane central pressure based on a maximum possible intensity argument
a_1, a_2, b_1, b_2	Location-dependent dimensionless scaling coefficients
g	Gravitational acceleration
m, m_2	Location-dependent dimensionless scaling coefficients
p	Probability density function
$p_1, p_2, p_3, p_4, q_1, q_2, q_3, q_4$	Dimensionless model fit coefficients
v_f	Hurricane forward speed near landfall
x	Location of interest measured on an axis running alongshore
x_o	x at the hurricane landfall position
x_{peak}	x at location of highest alongshore maximum surge
x'	Dimensionless alongshore function
α, β	Location-dependent dimensionless scaling coefficients
ε	Epistemic uncertainty in the surge response
ζ	Maximum hurricane surge at location of interest
ζ'	Dimensionless maximum hurricane surge
θ	Hurricane track angle with respect to the shoreline
λ	Ratio between relative alongshore position of highest surge and storm pressure radius
ρ	Water density
ϕ	Continuous SRF

1 Introduction and background

Accurate quantification of hurricane flooding probability is essential for coastal hazard risk assessment, coastal planning, and coastal engineering. Traditionally, hurricane surge probabilities are developed either by using historical surge elevations fit to parametric or nonparametric distributions or by using a suite of hypothetical surge events along with joint probability statistics. The historical population approach introduces significant statistical error, arising from sparse spatial and temporal occurrences of hurricane events (Agbley and Basco 2008; Irish et al. 2011a). Application of the joint probability method, while overcoming limitations of the historical population approach, has been difficult to apply due to the high computational burden imposed by high-resolution, physics-based

models. In this paper, the joint probability method with optimal sampling (JPM-OS) by using surge response functions (SRF), introduced in Resio et al. (2009) and Irish et al. (2009), is modified to improve the utility and accuracy of SRFs for hurricane surge estimation. Specifically, we investigate the sensitivity of hurricane surge to storm size and to regional bathymetric characteristics, namely continental shelf width.

The selected study area is the Texas, US coast (Fig. 1), which spans approximately 580 km from the US–Mexico border to the south to the Texas–Louisiana border to the northeast. This region is highly susceptible to hurricane activity and high surges. Most recently, Hurricane Ike (2008) generated storm surges in excess of 4 m in some locations along the Texas coast (East et al. 2008). Coastal Texas is low-lying and characterized by a system of coastal bays separated from the Gulf of Mexico by narrow barrier islands. Major metropolitan areas include the Cities of Houston and Galveston (between locations 3 and 4 on Fig. 1) and the City of Corpus Christi (between locations 1 and 2 on Fig. 1).

The strength of JPM-OS lies in the ability to quantify extreme-value flood statistics based on a wide range of hurricane possibilities while at the same time benefiting from the accuracy afforded by a limited, optimal sample of high-resolution, physics-based numerical simulations of storm surge. With the JPM-OS, Resio et al. (2009) assumed a continuous probability density function (p) to quantify return period (T_R) as follows:

$$T_R(\zeta) = \left\{ 1 - \int_{c_p} \int_{R_p} \int_{v_f} \int_{\theta} \int_{x_o} p\left(c_p, R_p, v_f, \theta, x_o\right) \left[H\left(\zeta - \left[\phi\left(x, c_p, R_p, v_f, \theta, x_o\right) + \varepsilon\right]\right)\right] \right.$$
$$\left. \times \, \mathrm{d}x_o \mathrm{d}\theta \mathrm{d}v_f \mathrm{d}R_p \mathrm{d}c_p \right\}^{-1} \tag{1}$$

where ζ is maximum hurricane surge at location of interest, c_p is hurricane central pressure near landfall, R_p is hurricane pressure radius near landfall (Thompson and Cardone 1996), v_f is hurricane forward speed near landfall, θ is hurricane track angle with respect to the shoreline, x_o is hurricane landfall location, H is the Heaviside function where $H(y) = 1$

Fig. 1 Location map. *Dotted and heavy solid lines* indicate hurricane tracks used in simulations, *solid circles* represent selected locations for surge response function development, and *dashed line* represents the 30-m depth contour. Mategorda Bay is just northeast of location 2
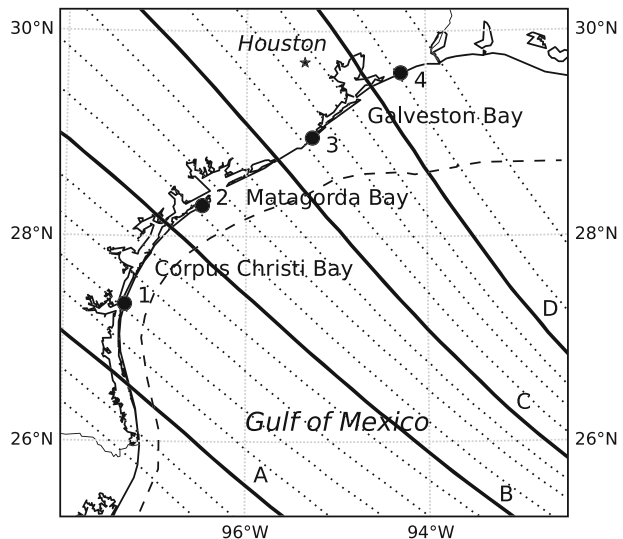
when $y \geq 0$ (here, this represents nonexceedance) and $H(y) = 0$ when $y < 0$, ϕ is a continuous SRF, x is location of interest, and ε is epistemic uncertainty in the surge response (Resio et al. 2009; Resio et al. in review).

Several approaches have been proposed for developing and interpolating from the optimal sample (e.g., Toro et al. 2010a, b; Condon and Sheng 2012), and Condon and Sheng (2012) presented a thorough review of these methods. Here, we focus on the use of continuous SRFs for functional interpolation. A main advantage of the SRF approach over other methods is in the use of dimensional analysis and physics-based arguments to develop the dimensionless SRF form. Since physical processes are considered directly, this approach helps to minimize interpolation error in portions of the parameter space characterized by significant changes in the surge response, for example, as Irish et al. (2009) showed for small storms making landfall near the location of interest. In Irish et al. (2009), three primary parameters contributing to storm surge were considered: storm central pressure, size, and landfall location; the SRFs were shown to be in the following dimensionless form:

$$\zeta'(x') = \frac{\rho g \zeta(x)}{P_{\text{far}} - c_p} + m(x) \left(\frac{P_{\text{far}} - c_p}{P_{\text{far}} - c_{p-\max}} \right) \tag{2a}$$

$$x' = \left(\frac{x - x_o}{R_p} - \lambda \right) - F \left(1 - \frac{R_p}{R_{\text{thres}}} \right) H \left(1 - \frac{R_p}{R_{\text{thres}}} \right) \tag{2b}$$

where

$$F \left(1 - \frac{R_p}{R_{\text{thres}}} \right) = \begin{cases} a_1 \left(1 - \frac{R_p}{R_{\text{thres}}} \right) + a_2 & \text{when } -\lambda \leq x' \leq 0 \\ b_1 \left(1 - \frac{R_p}{R_{\text{thres}}} \right) + b_2 & \text{when } 0 < x' < \lambda \\ 0 & \text{when } \lambda < |x'| \end{cases} \tag{2c}$$

$\zeta'(x')$ is dimensionless maximum hurricane surge, x' is a dimensionless alongshore function, ρ is water density, g is gravitational acceleration, x is location of interest measured on an axis running alongshore, P_{far} is the far-field barometric pressure, $c_{p\text{-max}}$ is a constant minimum possible hurricane central pressure based on a maximum possible intensity argument (e.g., Tonkin et al. 2000), and $m(x)$ is a location-specific dimensionless scaling coefficient, x_o is x at the hurricane landfall position, λ is a constant, R_{thres} is a constant, threshold value of R_p, and a_1, a_2, b_1, and b_2 are location-dependent scaling coefficients.

In Eq. 2a, the first term represents the first-order momentum balance, while the second term represents additional wind drag effects.

The SRF model given by Eq. 2 was developed through the analysis of high-resolution, physics-based storm surge simulations made with ADCIRC, a finite-element circulation model (e.g., Westerink et al. 2008) and considering four locations on the central Texas, US coast, in the vicinity of Matagorda Bay (near location 2 on Fig. 1). It was shown that SRFs given by Eq. 2 could be developed using just 25 % of the computational simulations typically required for application of a JPM approach; predictions with Eq. 2 reproduced maximum storm surge with root-mean-square errors less than 0.25 m (9 % of surge or less) and were highly correlated with simulated results, where R^2 was 0.94 or higher at all four locations. The SRF form in Eq. 2 has also been shown to perform well for predicting historical surges; Irish et al. (2011b) presented comparisons between observations and SRF predictions for five historical hurricanes impacting the Texas coast, showing that the SRFs

given by Eq. 2 provide reasonable predictions of surge magnitude and distribution along the coast.

While this initial SRF form works very well for the central Texas coast, it was found to be less accurate in other areas along the Texas coast (Fig. 2, locations 1, 3, and 4). Root-mean-square errors between the SRF-predicted surges by Eq. 2 and the ADCIRC-simulated surges are between 0.40 and 0.49 m, nearly twice that at central Texas locations (e.g., location 2 in Fig. 2). Percent errors at these locations are between 25 and 42 %. We will show that these inaccuracies arise primarily because of the relative importance of storm size and continental shelf width in these areas. In the following, we introduce the methods used to quantify the role of storm size and continental shelf geometry in storm surge generation. We then propose a modified SRF formulation that is more universally applicable along the open coast.

Fig. 2 Surge response functions (SRF; *left*) developed using Eq. 2 and SRF-predicted versus ADCIRC-simulated maximum surge for selected locations (see Fig. 1)
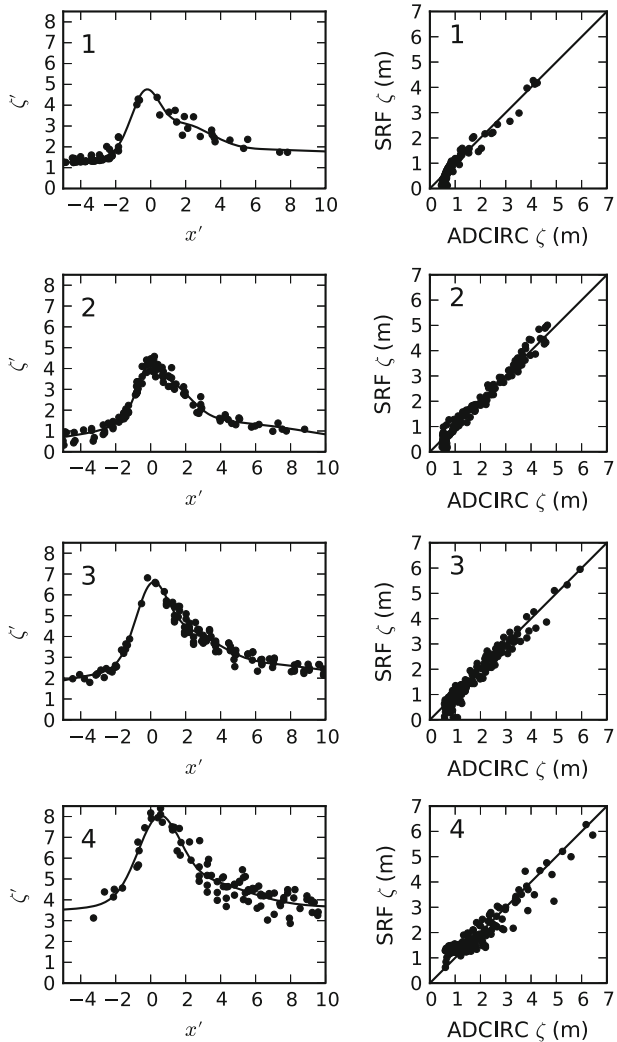
2 Methods

In this paper, we follow the methods presented in Irish et al. (2009); these are summarized here. Storms surges along the Texas coastline were computed using the finite-element hydrodynamic model ADCIRC (e.g., Westerink et al. 2008). In the two-dimensional, depth-integrated form employed here, ADCIRC is used to solve the shallow water mass and momentum balances. The ADCIRC model domain included the entire Gulf of Mexico and the North Atlantic basin to 60°W longitude, and the domain is highly resolved, as fine as 50 m, throughout the Texas nearshore and inland bay system (see Irish et al. 2009). The grid extends onshore to elevations on the order of 25 m above mean sea level. Standard model settings were employed, and a model time step of 0.5 s was used. The model setup was validated for storm surge simulation, demonstrating accuracy within 0.30 m of observed surges at most locations (e.g., U.S. Army Corps of Engineers 2006). ADCIRC was forced with wind and barometric pressure fields only. Tides and ocean wave setup, both of which can add to storm flood levels, were omitted for simplification. Astronomical tides can typically be considered as a linear addition to surge level in most open-coast locations, and added surge level by wave-induced setup, which typically contributes less to total flood level than wind surge for high surge events, is anticipated to scale in a similar manner as the wind surge considered here.

Wind and barometric pressure fields were developed with a coupled hurricane vortex, planetary boundary layer model (PBL; Thompson and Cardone 1996). To force the PBL model, storm position, central pressure, storm size, storm forward speed, and peakedness (Holland 1980 B) were specified at 6-h intervals along the hurricane's track. With the PBL model, wind and pressure fields at 15-min intervals, and with 2-km resolution in the central part of the hurricane, were generated then used to force the ADCIRC simulations. To focus the analysis on surge response as a function of landfall position, central pressure, and storm size, only hurricanes approaching the Texas coast from the southeast at 5.7 m/s were considered, representing one typical path and an average forward speed for hurricanes impacting the northern Gulf of Mexico coast (Dorst 2007). For the Texas coast, the selected track orientation corresponds to track angles between −45° and +10° with respect to shore normal (positive is counterclockwise). Meteorological parameters for selected

Table 1 Meteorological parameters near landfall for selected historical storms impacting Texas [from Landsea et al. (2005) unless otherwise noted]

Hurricane name (date)	Latitude/longitude [L_{30} (km)]	c_p (mb)	R_{max} (km)	V_f (m/s)	θ (°)	Maximum observed surge (m)[f]
Audrey (1957)	29.7N/93.7W [105]	946	46	6	−10	3.4–3.8
Carla (1961)	28.0N/96.4W [30]	936[a]	56[a]	3	−10	3.3–3.7
Beulah (1967)	25.9N/97.2W [20]	950	46[a]	5	−50	2.4–2.9
Celia (1970)	27.8N/97.1W [25]	944	17[a]	6	+5	2.7–2.8
Allen (1980)	26.1N/97.2W [20]	945	37[a]	3	−35	2.1–3.7
Alicia (1983)	28.9N/95.0W [50]	962[b]	20[b]	3	−15	3.7
Bret (1999)	26.9N/97.4W [20]	953[a]	19[a]	4	−30	0.9–1.5
Rita (2005)	29.4N/93.6W [100]	937[c]	30[c]	5	+15	3.0–4.6 (Louisiana)
Ike (2008)	29.1N/94.6W [90]	950[d]	195[e]	4	+5	4.8–5.9

[a] U.S. Army Corps of Engineers (2006); [b] Powell (1987); [c] Powell and Reinhold (2007); [d] Berg (2009); [e] Irish et al. (2011b); [f] Irish et al. (2008)

historical events are given in Table 1. As this table shows, the selected parameter range for study is representative of hurricanes impacting the region.

While forward speed and track angle indeed can influence surge magnitude, in most cases, its influence is small with respect to other factors (e.g., Irish et al. 2008; Rego and Li 2009; Niedoroda et al. 2010; Toro et al. 2010b). Irish et al. (2008) showed via idealized computational simulations that peak surge varied 15–20 % when forward speed was changed by 50 %, for storms tracking over moderate to narrow continental shelf widths; the variation was shown to be minimal for storms tracking over wide shelves. In this same study, the authors also showed that peak surge varied by no more than 10 % for track angles between −50° and +30°, with respect to surge when the track angle is 0° (shore normal). Two-thirds of these simulations yielded surges within 0.20 m (4 %) of the shore-normal track value. Analysis of the storm surge simulations of Udoh and Irish (2011) for the entire Texas coast shows that on average surge varies by 0.35 m, when comparing surge from tracks approaching from the south-southeast and from the east-southeast with surge from tracks approaching from the southeast. In contrast, below we will show that the surge variations due landfall location are on the order of 1 m or more.

It was shown that the SRF form in Eq. 2 may be specified with an optimal sample of storms, specifically by limiting the number of combinations of central pressures, storm sizes, and tracks considered. Based on this finding, an optimal sample of 145 storms, distributed over 18 tracks (Fig. 1), were simulated here to represent the storm parameter space for the entire Texas coast, about 600 km. The parameters c_p and R_p were varied from 900–960 mb and 11–66 km, respectively; two to nine (c_p, R_p) combinations were simulated on each track.

3 Simulation results

The simulated hurricane surges for the Texas coast were analyzed to assess the relative impact of continental shelf width and storm size on maximum surge. Figure 3 shows selected results, where maximum surge at the shoreline is plotted versus alongshore distance from landfall position. Three main characteristics are revealed by these results. First, when storm size and central pressure are held constant, as landfall position changes from southwest to northeast, maximum surge magnitude increases along much of the coast. At the alongshore location of highest surge, surge varies by almost 2 m, depending on landfall position. The asymmetry in surge response about the location of highest surge also becomes more pronounced as landfall position moves northward. On average, simulated surge magnitudes at location 4 (see Fig. 1) are 1.2 m higher than those at location 1, when central pressure, storm size, and relative track position $(x - x_o)$ are held constant. Second, the relative distance between landfall position and alongshore location of highest maximum surge is smaller for storms making landfall along the lower Texas coast and larger for storms making landfall along the upper Texas coast. These changes in surge magnitude and alongshore distribution are consequences of the relatively large region over which surge may be generated on the upper Texas coast, as is characterized by a wide continental shelf width, with respect to the lower Texas coast (see Fig. 1).

Third, when central pressure is held constant, for a given landfall position along the upper Texas coast, the maximum surge increases as storm size increases (Fig. 3). The relative increase in surge with storm size is more dramatic at and to the north of the alongshore location of highest maximum surge. Thus, increasing storm size also adds to the asymmetry in alongshore surge response. For storms making landfall on the lower

Fig. 3 Maximum ADCIRC-simulated surge versus alongshore distance for selected tracks (*solid line tracks* labeled A through D in Fig. 1) when $c_p = 900$ mb and $R_p = 28$ km (*blue*) and 40 km (*black*). Simulated surges were taken just offshore of the mean sea-level shoreline. Alongshore distance is specified such that $x - x_o = 0$ corresponds to storm landfall position, where positive $x - x_o$ is toward the north. The alongshore position x spans the entire Texas coast, from the US–Mexico border to the Texas–Louisiana border
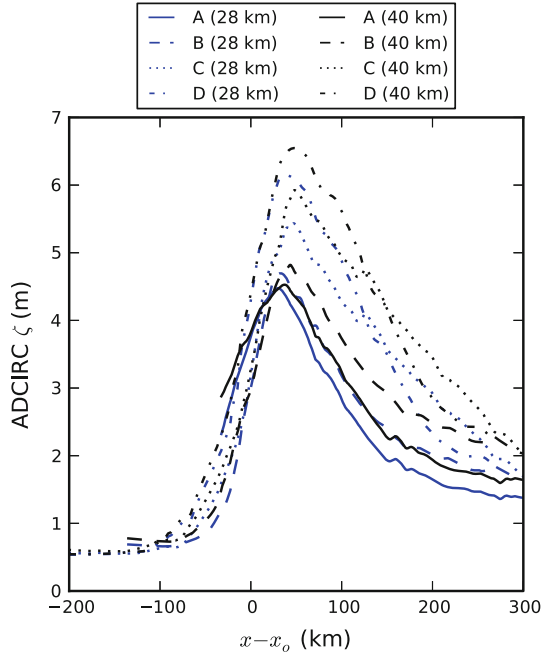
Texas coast, the impact of storm size on maximum surge is small. This highlights the relative importance of storm size as a function of regional characteristics such as continental shelf width (Irish et al. 2008, 2011b; Irish and Resio 2010).

These findings suggest that maximum hurricane surge and its distribution along the coast additionally scale with both storm size and continental shelf width and that the relative importance of these parameters increases with increasing continental shelf width.

4 Improved surge response function formulation

In order to improve the SRF formulation to ensure better performance in this region, a new parameter is introduced to account for the role of continental shelf width on surge generation. In addition, we will introduce the storm size parameter into the dimensionless surge. As Fig. 3 shows, continental shelf width in the vicinity of storm landfall plays an important role in the location of highest alongshore maximum surge. For discussion and analysis here, we consider cross-shore distance between the shoreline and the 30-m depth contour, L_{30}, to be representative of the continental shelf width relevant for surge generation (Fig. 1; Irish and Resio 2010). The parameter λ in Eq. 2b physically represents the ratio between the alongshore distance between storm landfall and highest alongshore maximum surge ($x_{peak} - x_o$) and hurricane pressure radius:

$$\lambda = \frac{x_{peak} - x_o}{R_p} \tag{3}$$

This parameter was estimated to be constant at $\lambda = 0.87$ for hurricanes impacting the central Texas coast, in the vicinity of Matagorda Bay. In contrast, Fig. 3 suggests that λ is not constant, but varies with continental shelf width.

A 90-km alongshore moving average was applied to the simulated data to obtain spatially dependent estimates of λ; in general, storms making landfall on the upper Texas coast are characterized by larger values of λ, whereas storms making landfall on the lower Texas coast are characterized by smaller values. Data analysis revealed a strong linear correlation between λ and L_{30}, when L_{30} is less than 40 km (Fig. 4). For larger L_{30}, λ approaches a constant value of 0.88. Curve fitting by linear regression yields the following relationship for the Texas coast:

$$\lambda(x_o) = \begin{cases} 0.05L_{30}(x_o) - 0.70 \text{ when } L_{30}(x_o) < 40 \text{ km} \\ \frac{2.03}{L_{30}(x_o) - 31.4} + 0.88 \text{ when } L_{30}(x_o) \geq 40 \text{ km} \end{cases} \quad (4)$$

where L_{30} is in km. The location of highest surge along the lower Texas coast linearly increases with continental shelf width. In contrast, along the upper Texas coast, the wider shelf results in relatively more surge generation to the north, thereby shifting the location of highest alongshore surge northward. Along the upper Texas coast, λ approaches a constant value of 0.88. The additional surge and shift in position of highest alongshore surge along the upper Texas coast, namely an increase in λ, may arise from a combination of increased wind surge and Eckman setup, as occurred during Hurricane Ike in 2008 (Kennedy et al. 2011). On the Texas coast, λ has a maximum of 1.15 about halfway between Matagorda and Galveston, and this is a somewhat unexpected finding. In locations with more gradually varying continental shelf width, we would expect a monotonic increase in λ, up to a maximum value near unity, with L_{30}. The localized increase in λ in this region arises because the continental shelf rapidly widens and changes orientation (see Fig. 1). Specifically, we hypothesize that surge generated by onshore-directed winds interacts with surge generated by winds acting in the alongshore direction along the portion of the continental shelf to the north of this location. A λ value greater than unity suggests that at this location, the alongshore-generated portion of the surge makes a significant contribution.

Figure 3 also showed that both storm size and continental shelf width impact the degree of asymmetry that is evident in alongshore surge distribution. The role of storm size and

Fig. 4 Ratio between ADCIRC-simulated distance from landfall to highest alongshore maximum surge and storm size, λ, versus cross-shore distance between shoreline and 30-m depth contour, L_{30}. Each data point shown represents a 90-km moving average value
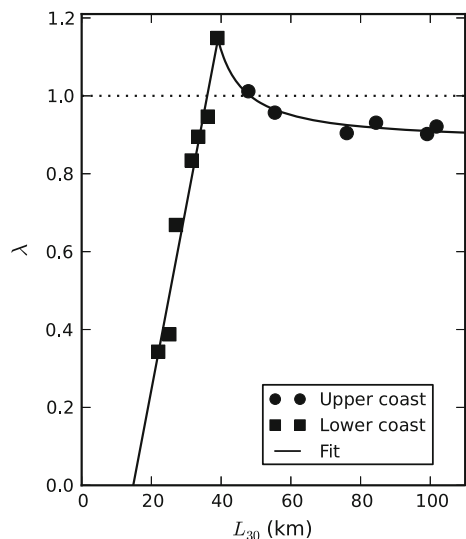
continental shelf width on this asymmetry can also be seen in the preliminary dimensionless scaling results (Fig. 5, top pane). Here, we consider the ratio R_p/L_{30}, where larger values of R_p/L_{30} represent relatively larger storms making landfall over relatively narrow continental shelves. As Fig. 5 (top pane) shows for the northernmost location (see Fig. 1), larger values of R_p/L_{30} result in narrower dimensionless surge distributions in the alongshore region to the north of highest alongshore surge. No significant trend was observed in the alongshore region to the south of highest alongshore maximum surge, consistent with the dimensional results in Fig. 3. In addition, at locations to the south, when $L_{30} < 40$ km, no significant trend with R_p/L_{30} is evident; this is expected since in this region, wind surge generation is limited owing to predominantly offshore-directed winds as the storm passes over the continental shelf. We introduce the following correction into the dimensionless alongshore variable in order to account for this asymmetry:

$$
\begin{aligned}
x' = {} & \frac{(x - x_o)}{R_p} - \lambda(x_o) + cH\left(\frac{(x - x_o)}{R_p} - \lambda(x_o) - 1\right)H\left(\frac{L_{30}}{L_{30-\text{ref}}} - 1\right)\left(\frac{R_p}{L_{30}}\right) \\
& - F\left(1 - \frac{R_p}{R_\text{thres}}\right)H\left(1 - \frac{R_p}{R_\text{thres}}\right)
\end{aligned}
\tag{5}
$$

where c is a dimensionless regional scaling constant and $L_{30\text{-ref}}$ is a reference value of L_{30}. For the Texas coast, $c = 0.75$ and $L_{30\text{-ref}} = 40$ km; these values were determined by inspection. Figure 5 (bottom pane) shows the resulting shift and general convergence of the data in the preliminary dimensionless space.

Irish and Resio (2010) argued that both storm size and the size of the shallow region, specifically the continental shelf region, can limit surge magnitude. In the case where storm size is smaller than the continental shelf region over which the storm passes, the wind field size effectively limits surge generation. On the other hand, in the case where the storm size is larger the continental shelf region, the size of the continental shelf effectively limits surge generation. Thus, surge magnitude can be expected to scale with R_p/L_{30}. Figure 6 shows simulated highest alongshore maximum surge versus R_p/L_{30}, showing that surge decreases with increasing R_p/L_{30} in an almost linear fashion.

To account for the relative roles of storm size and continental shelf width in the dimensionless surge magnitude variable, the ratio R_p/L_{30} is introduced into Eq. 2a as follows:

$$
\zeta' = \frac{\gamma \zeta}{\Delta p} + m_2(x, x')\left(\frac{P_\text{far} - c_p}{P_\text{far} - c_{p-\text{max}}}\right)^{\alpha(x,x')}\left(\frac{R_p/L_{30}(x_o)}{[R_p/L_{30}]_\text{ref}}\right)^{\beta(x,x')}
\tag{6}
$$

where m_2, α, and β are dimensionless scaling coefficients varying by location and x' as follows:

$$
[m_2(x, x'), \alpha(x, x'), \beta(x, x')] = \begin{cases} [m_{2L}(x), \alpha_L(x), \beta_L(x)] & \text{for } x' < 0 \\ [m_{2R}(x), \alpha_R(x), \beta_R(x)] & \text{for } x' \geq 0 \end{cases}, \text{ and}
$$

$[R_p/L_{30}]_\text{ref}$ is a regional constant representing the maximum value of R_p/L_{30}.

For the Texas coast, $c_{p\text{-max}}$ and $[R_p/L_{30}]_\text{ref}$ are taken as 870 mb (Tonkin et al. 2000) and 3.5, respectively. The scaling coefficients m_2, α, and β are determined by linear regression (Table 2), where values for α and β are limited to $0 \leq \alpha$ or $\beta \leq 1$. For the Texas coast, the coefficient m_2 varies between 0.43 and -17.86. Separate specification of these three scaling coefficients for storms with $x' < 0$ (L) and with $x' \geq 0$ (R) creates an SRF that better captures differing surge patterns for each domain. In the range of $x' \geq 0$, the surge

Fig. 5 Alongshore asymmetry in surge distribution in the preliminary dimensionless space before (*top pane*) and after (*bottom pane*) modification of the dimensionless alongshore axis using the ratio between storm size, R_p, and cross-shore distance between shoreline and 30-m depth contour, L_{30}
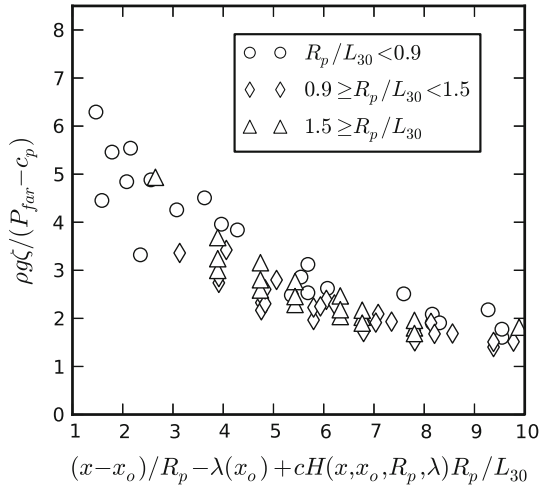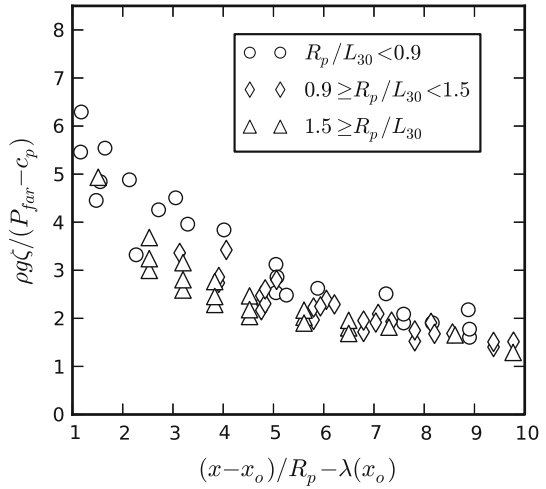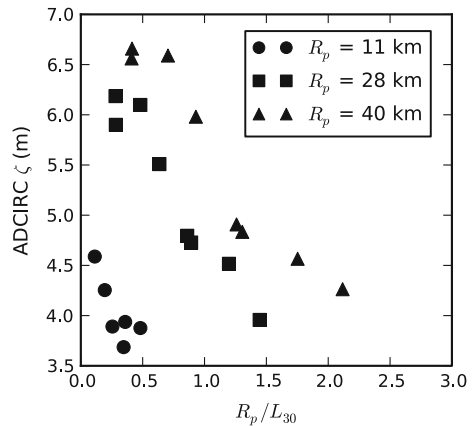

Fig. 6 Ratio between storm size, R_p, and cross-shore distance between shoreline and 30-m depth contour, L_{30}, versus highest alongshore maximum ADCIRC-simulated surge, ζ, for simulations when $c_p = 900$ mb

response is typically directly generated by strong onshore winds, leading to larger surge magnitudes particularly when L_{30} is large. In the range of $x' < 0$, as the storm passes over the continental shelf, this region is typically exposed to offshore-directed winds, thereby leading to lower surge magnitudes and limited alongshore extent of high surge.

4.1 Performance

The dimensionless SRF derived by using Eqs. 5 and 6 is shown for selected locations in Fig. 7. The following two-term exponential equation was fit to the dimensionless data to develop a model for the SRF:

$$\zeta' = \begin{cases} p_1 \exp(p_2 x') + p_3 \exp(p_4 x') & \text{when } x' < 0 \\ q_1 \exp(q_2 x') + q_3 \exp(q_4 x') & \text{when } x' \geq 0 \end{cases} \tag{7}$$

where p_1, p_2, p_3, p_4, q_1, q_2, q_3, and q_4 are dimensionless model fit coefficients determined by linear regression (Table 3).

As Fig. 7 (left panes) shows, the simulated surge data collapse in this new dimensionless form, and the SRF model given by Eq. 7 well represents the dimensionless data, with R^2 of 0.95 or better at all locations. The SRF model given by Eq. 7 and developed from Eqs. 5 and 6 also performs well in predicting surge; the error statistics in Table 4 show a marked improvement in SRF model skill with respect to the formulation based on Eq. 2. Mean errors are between -0.03 and 0.01 m, indicating no significant bias in surge predictions, while root-mean-square errors are 0.22 m or better. This represents a 50–70 % reduction in root-mean-square error for locations where the SRF was not well represented by Eq. 2, namely locations 1, 3, and 4; the new formulation yields an improvement of 30 % at location 3. Similarly, the new SRF model measurably improves correlation between simulated and predicted surges, with R^2 of 0.97 or better at all locations. Overall, this new SRF model yields surge estimates with absolute percent errors of less than 10 %, with respect to high-resolution simulations.

To further assess predictive skill, we compared estimates using the new SRF model with water-level gauge and high water mark observations made during four historical hurricanes (see Irish et al. 2011b for observed data). Mean absolute error is 0.42 m. In addition to the uncertainty known to accompany high water mark observations, much of this error can be explained by the omission of wave setup in the current SRF model. Thus, we may interpret the comparison between the SRF model and field data as being quite good.

Table 2 Dimensionless scaling coefficients for Eqs. 5, 6, and 7 for selected locations (see Fig. 1 for locations)

Location	a_1	a_2	b_1	b_2	x' range	α	β	m_2
1	0.00	0.00	0.00	-0.94	$x' < 0$	0.50	0.10	-2.46
					$x' \geq 0$	0.10	0.05	0.68
2	1.58	-0.49	0.00	0.00	$x' < 0$	0.10	0.05	-2.71
					$x' \geq 0$	0.15	0.05	-3.30
3	0.00	0.00	0.00	0.00	$x' < 0$	0.20	0.00	-3.71
					$x' \geq 0$	0.00	1.00	0.43
4	0.00	0.00	0.00	-0.41	$x' < 0$	1.00	0.10	-2.52
					$x' \geq 0$	0.05	0.00	-17.86

Fig. 7 Improved surge response functions (SRF; *left*) developed using Eqs. 5, 6, and 7 and SRF-predicted versus ADCIRC-simulated maximum surge for selected locations (see Fig. 1)
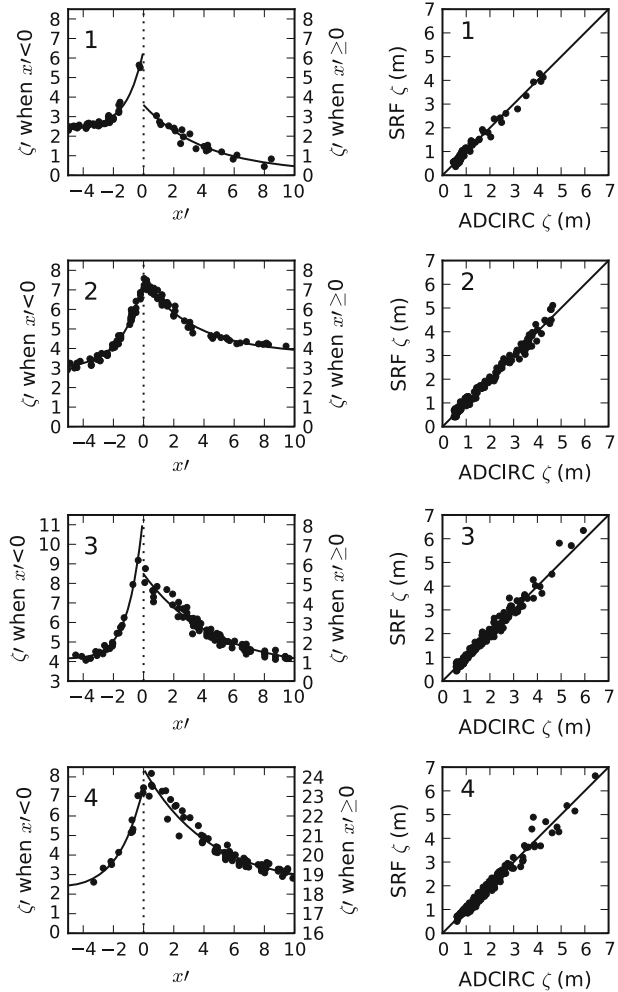
Table 3 Dimensionless model coefficients for Eq. 7 for selected locations (see Fig. 1 for locations)

Location	R^2 (p/q)	p_1	p_2	p_3	p_4	q_1	q_2	q_3	q_4
1	0.97/0.94	2.4	6.3e − 3	4.0	9.0e − 1	3.1	2.6e − 1	4.7e − 1	−7.4e − 2
2	0.98/0.98	3.0	2.0e − 3	4.5	6.9e − 1	3.6	−3.1e − 1	4.0	−4.7e − 3
3	0.99/0.96	4.0	−7.8e − 3	7.7	1.0	4.8	−2.2e − 1	6.6e − 1	−2.9e − 3
4	0.97/0.97	1.4	−7.3e − 2	6.1	5.4e − 1	5.9	−2.4e − 1	19	−4.8e − 4

4.2 Suitability of formulation for application in other locations

The above SRF formulation considers surge generation in regions with continuous coasts. It is anticipated that the general SRF form in Eqs. 5 and 6 will hold in these environments. While central pressure, storm size, landfall location, and continental shelf width are expected to impact surge generation and distribution along any arbitrary continuous coast,

Table 4 Error statistics for maximum surge estimation with original and improved surge response functions (see Fig. 1 for locations)

Location	Root-mean-square error (m)		Mean error (m)		R^2	
	Original	New	Original	New	Original	New
1	0.40	0.11	0.20	0.00	0.85	0.98
2	0.24	0.16	0.03	−0.01	0.97	0.99
3	0.49	0.19	0.16	−0.03	0.87	0.97
4	0.42	0.22	−0.03	0.01	0.88	0.97

the exact SRF shape will vary from location to location. Thus, site-specific field data and/or high-resolution computational simulations must be analyzed to assess local fit coefficients. Furthermore, due to the unique curvature of the continental shelf with respect to the coastline orientation along the Texas coast, the relationship between the coefficient λ and L_{30} should be reviewed separately for each site.

The SRF form presented here may not be suitable in locations without a continuous coast; for example, for surge generation near the southern tip of Florida or in the Caribbean Islands. Along these discontinuous coasts, surge is released around the peninsula tip or edges of the islands, thereby violating the key assumption that alongshore surge distribution will be governed by storm size and continental shelf width alone.

5 Summary and conclusions

Using dimensionless scaling, a general form for estimating extreme hurricane surges along a continuous coast was developed. This SRF form accounts for the primary hurricane parameters impacting surge generation, namely landfall position, central pressure, and storm size. We have shown that the coupled impact of continental shelf width and storm size on both surge magnitude and its alongshore distribution is captured by the new dimensionless SRF form. The SRF models for the Texas coast are highly correlated with simulated surges, and these models produce maximum surge estimates with unbiased and minimal error.

This SRF model may be coupled with joint probability statistics to allow specification of continuous probability density functions in order to assess extreme-value and forecast surge statistics (Irish et al. 2011b) needed for coastal planning, design, and evacuation. Because of the physical representation and dimensionless scaling, just a small subset of detailed, high-resolution surge simulations are needed to develop the SRFs, which in turn allows functional interpolation of all hurricane possibilities needed for developing continuous probability density functions. The SRF models may be used to identify which suite of storm parameters results in specific surge levels, for example, which contribute to the 100-year surge event. The SRF model may further be used to support high-risk design decisions, for example, selecting locations for nuclear power plants, by allowing identification of the worst-case hurricane surge condition. While we used ADCIRC to develop the simulation dataset for the Texas coast, SRF models may be developed from any existing hurricane surge simulation or surge measurement dataset.

Finally, for more robust applications, the SRF form presented here should be expanded to account for the relative roles of storm forward speed and approach angle in surge generation, as well as flood contributions by wave setup, inland runoff and river discharge,

and astronomical tides. We expect that these physical processes will exhibit clear patterns that can be readily incorporated into the SRF form presented here. In addition, local natural and manmade landscape features such as ridges, rivers, and levees add an additional challenge for SRF application. Analysis of high-resolution storm surge simulations that resolve these features will help to quantify their impact on the SRF form and prediction accuracy.

References

Agbley SK, Basco DR (2008) An evaluation of storm surge frequency-of-occurrence estimator. In: ASCE (ed) Solutions to coastal disasters, Oahu, Hawaii. ASCE, pp 185–197

Berg R (2009) Tropical cyclone report Hurricane Ike (AL092008). National Hurricane Center, Miami, FL, p 55, September 2008

Condon AJ, Sheng YP (2012) Optimal storm generation for evaluation of the storm surge inundation threat. Ocean Eng 43:13–22. doi:10.1016/j.oceaneng.2012.01.021

Dorst N (2007) What is the average forward speed of a hurricane? In Hurricane research division frequently asked questions. National Oceanic and Atmospheric Administration. http://www.aoml.noaa.gov/hrd/tcfaq/G16.html

East JW, Turco MJ, Mason RR (2008) Monitoring inland storm surge and flooding from Hurricane Ike in Texas and Louisiana, September 2008. U.S. Geological Survey Open File Report, 2008–1365, p 38

Holland GJ (1980) An analytic model of the wind and pressure profiles in hurricanes. Mon Weather Rev 108:1212–1218. doi:10.1175/1520-0493(1980)108<1212:AAMOTW>2.0.CO;2

Irish JL, Resio DT (2010) A hydrodynamics-based surge scale for hurricanes. Ocean Eng 37(1):69–81. doi:10.1016/J.Oceaneng.2009.07.012

Irish JL, Resio DT, Ratcliff JJ (2008) The influence of storm size on hurricane surge. J Phys Oceanogr 38(9):2003–2013. doi:10.1175/2008jpo3727.1

Irish JL, Resio DT, Cialone MA (2009) A surge response function approach to coastal hazard assessment. Part 2: quantification of spatial attributes of response functions. Nat Hazards 51(1):183–205. doi:10.1007/S11069-009-9381-4

Irish JL, Resio DT, Divoky D (2011a) Statistical properties of hurricane surge along a coast. J Geophys Res [Oceans] 116:C10007. doi:10.1029/2010JC006626

Irish JL, Song YK, Chang K-A (2011b) Probabilistic hurricane surge forecasting using parameterized surge response functions. Geophys Res Lett 38:L03606. doi:10.1029/2010GL046347

Kennedy AB, Gravois U, Zachry BC, Westerink JJ, Hope ME, Dietrich JC, Powell MD, Cox AT, Luettich RA, Dean RG (2011) Origin of the Hurricane Ike forerunner surge. Geophys Res Lett 38:L08608. doi:10.1029/2011gl047090

Landsea CW, Anderson C, Charles N, Clark G, Dunion J, Fernandez-Partagas J, Hungerford P, Neumann C, Zimmer M (2005) The Atlantic hurricane database re-analysis project: documentation for 1951–1910 alterations and additions to the HURDAT database. In: Murnane RJ, Liu K-B (eds) Hurricanes and typhoons: past, present, and future. Columbia University Press, New York, pp 178–221

Niedoroda AW, Resio DT, Toro G, Divoky D, Reed C (2010) Analysis of the coastal Mississippi storm surge hazard. Ocean Eng 37(1):82–90. doi:10.1016/j.oceaneng.2009.08.019

Powell MD (1987) Changes in the low-level kinematic and thermodynamic structure of Hurricane Alicia (1983) at landfall. Mon Weather Rev 115:75–99

Powell MD, Reinhold TA (2007) Tropical cyclone destructive potential by integrated kinetic energy. Bull Am Meteorol Soc 88(4):513–526

Rego JL, Li CY (2009) On the importance of the forward speed of hurricanes in storm surge forecasting: a numerical study. Geophys Res Lett 36:L07609. doi:10.1029/2008gl036953

Resio DT, Irish J, Cialone M (2009) A surge response function approach to coastal hazard assessment—part 1: basic concepts. Nat Hazards 51(1):163–182. doi:10.1007/S11069-009-9379-Y

Resio DT, Irish JL, Westerink JJ, Powell N (in review) The effect of uncertainty on estimates of hurricane surge hazards. Natural Hazards

Thompson EF, Cardone VJ (1996) Practical modeling of hurricane surface wind fields. J Waterw Port Coast Ocean Eng ASCE 122(4):195–205

Tonkin H, Holland GJ, Holbrook N, Henderson-Sellers A (2000) An evaluation of thermodynamic estimates of climatological maximum potential tropical cyclone intensity. Mon Weather Rev 135:746–764

Toro GR, Niedoroda AW, Reed CW, Divoky D (2010a) Quadrature-based approach for the efficient evaluation of surge hazard. Ocean Eng 37(1):114–124. doi:10.1016/j.oceaneng.2009.09.005

Toro GR, Resio DT, Divoky D, Niedoroda AW, Reed C (2010b) Efficient joint-probability methods for hurricane surge frequency analysis. Ocean Eng 37(1):125–134. doi:10.1016/j.oceaneng.2009.09.004

Udoh IE, Irish JL (2011) Improvements in hurricane surge response functions: Incorporating the effects of forward speed, approach angle, and sea level rise. In: Proceedings of the 1st international conference on vulnerability and risk analysis and management, College Park, MD

U.S. Army Corps of Engineers (2006) Performance evaluation of the New Orleans and southeast Louisiana hurricane protection system draft final report of the Interagency Performance Evaluation Task Force. U.S. Army Corps of Engineers

Westerink JJ, Luettich RA, Feyen JC, Atkinson JH, Dawson C, Roberts HJ, Powell MD, Dunion JP, Kubatko EJ, Pourtaheri H (2008) A basin- to channel-scale unstructured grid hurricane storm surge model applied to southern Louisiana. Mon Weather Rev 136(3):833–864. doi:10.1175/2007mwr1946.1